Anal. Chem. **1994**, *66*, 2552–2560

Second-Order Fiber Optic Heavy Metal Sensor Employing Second-Order Tensorial Calibration

Zhihao Lin, Karl S. Booksh, Lloyd W. Burgess, and Bruce R. Kowalski*

Center for Process Analytical Chemistry, Department of Chemistry, BG-10, University of Washington, Seattle, Washington 98195

A fully selective and versatile fiber optic heavy metal sensor based on the concept of second-order instrumentation has been fabricated and evaluated. This sensor uses chemically facilitated Donnan dialysis as the means of temporal species discrimination and reagent-assisted spectroscopy for spectral species discrimination. The signals in both orders (time and wavelength) are combined and analyzed with second-order tensorial analysis algorithms—generalized rank annihilation method (GRAM) and trilinear decomposition (TLD)—in order to extract the information of analytes form the sensor responses that are interfered by unknown interferents. Principal component analysis (PCA) is used to evaluate sensor characteristics. With second-order calibration, the sensor can measure Pb(II) or Cd(II) in the presence of other interfering transition metal ions. The prediction accuracy is affected by the response linearity of the sensor and the competition effect of co-existing cations with the analyte ions in the ion-exchange process. The specificity of the sensor can be easily switched from Pb(II) measurement into Cd(II) measurement by just changing the calibration standard. The sensor was also tested with "real-world" samples. With the stopped-flow preconcentration measuring mode, the sensor gains in sensitivity so that low concentration Pb(II) in tap water and lake water samples can be measured. For tap water samples, the sensor agrees with the graphite furnace atomic absorption (GFAA) verification very well. Due to complexation of Pb(II) in the lake water samples, some complexed Pb(II) ions are rejected by the cation-exchanging membrane, causing the sensor results to be lower than the GFAA data.

Increasing the measurement dimensionality, that is, the order of analytical instrumentation is an attractive approach to obtain substantial improvement of analytical capability. A conventional zero-order device, for example, an ion-selective electrode, must be specific for only one analyte. Quantitation is biased if another constituent in the sample matrix possesses characteristics similar to the analyte that results in an instrument response. Even worse, there is no evidence to let the analyst know that the measurement has been biased. This problem can be addressed by a first-order device, e.g., a spectrometer, which utilizes an analyte's multiplexed characteristics in one domain (i.e., absorbance at different wavelengths). For this device to work, a calibration model that includes the spectra of the analyte and all interfering species must be established. Multicomponent analysis and outlier detection are possible.[1,2] However, prediction will be successful only if there is no unexpected interferent in the sample matrix. Otherwise, erroneous prediction will occur. This problem is eliminated with second-order instrumentation. Second-order hyphenated instruments are two analytical mechanisms linked in series such that the signal of the later instrument is modulated by the first device. This type of instrument utilizes an analyte's characteristics in two independent domains, for example, the diffusivities and the spectral absorptivities in HPLC-UV measurements. For each measurement, a second-order instrument generates a data matrix. For a bilinear second-order device, that is, where the instrument response for the analyte is a rank one matrix, the calibration can be carried out using only one standard consisting of just the analyte of interest.[3] Prediction is robust to the presence of uncalibrated interferents. Since, in many cases, knowing all potential interferents and including these variations into the calibration model is very difficult, the so called "second-order advantage" is significant.

Modern laboratory analytical chemistry has benefited from the advance toward higher order instrumentation.[4-10] However, to some degree, an increasingly important field—in situ chemical analysis—has been left behind. Most in situ measurements rely on zero-order sensors and some first-order spectral probes. It is in this area where the second-order advantage is extremely important because of unpredictable changes in sample matrix composition. Therefore, the concept of second-order instrumentation in in situ chemical analysis has broad applicability. In many respects, this is not just a simple conceptual extension of laboratory instrumentation to the chemical sensor area. Limited by the requirements of cost, reliability, and physical size, researchers must use some simple, dedicated mechanisms to make second-order sensors. This opens a vast research area for sensor researchers and chemometricians, because these mechanisms usually do not exhibit comparable performance with their sophisticated laboratory counterparts, and more complicated calibration algorithms are needed to deconvolute the often collinear or nonlinear signal brought by the second-order sensors.

In this paper, we present a second-order fiber optic heavy metal sensor combining a chemically facilitated Donnan

(1) Sanchez, E.; Kowalski, B. R. *J. Chemom.* **1988**, *2*, 247–63.
(2) Gemperline, P. J. *J. Chemom.* **1989**, *3*, 549–68.
(3) Sanchez, E.; Kowalski, B. R. *J. Chemom.* **1988**, *2*, 265–80.
(4) Hirschfeld, T. *Anal. Chem.* **1980**, *52*, 297A.
(5) Burdick, Q. S.; Tu, X. M.; McGown, L. B.; Millican, D. W. *J. Chemom.* **1990**, *4*, 15–28.
(6) Hsu, J. *Anal. Chem.* **1992**, *64*, 434–43.
(7) Spraul, M.; Hofmann, M.; Dvortsak, P.; Nicholson, J.; Wilson, I. D. *Anal. Chem.* **1993**, *65*, 327–30.
(8) Bailey, W. I.; Kotz, A. L.; McDaniel, P. L.; Parees, D. M.; Schweighhart, F. K.; Yue, H. J. *Anal. Chem.* **1993**, *65*, 752–8.
(9) Takatera, K.; Watanabe, T. *Anal. Chem.* **1993**, *65*, 759–62.
(10) Lemmo, A. V.; Jorgenson, J. W. *Anal. Chem.* **1993**, *65*, 1576–81.

0003-2700/94/0366-2552$04.50/0

dialysis device developed by Lin and Burgess[11] with a low-cost, portable photodiode array spectrometer. The sensor is specific for measuring Pb(II) or Cd(II) in aqueous samples. Since it is important to monitor the heavy metal ions in environmental protection, devices capable of in situ, distributed measurement are highly desired. Atomic absorption/emission spectrophotometric methods are sensitive, selective, and accurate to measure metal ions, but they are not practical for in situ, distributed measurements because of high instrumentation and operation costs as well as the requirement of sample pretreatment in many cases. Ion-selective electrodes are inexpensive and easy to use and, hence, are suitable for in situ measurement. However, in spite of a great deal of research in this area, recently developed lead and cadmium ion-selective electrodes still lack selectivity and long-term stability.[12-15] Second-order instrumentation provides a new approach to solve the selectivity vs stability dilemma. Semiselective but stable membranes can be used to improve the long-term stability of the sensor whereas the selectivity is compensated by the multiwavelength detection and second-order calibration.

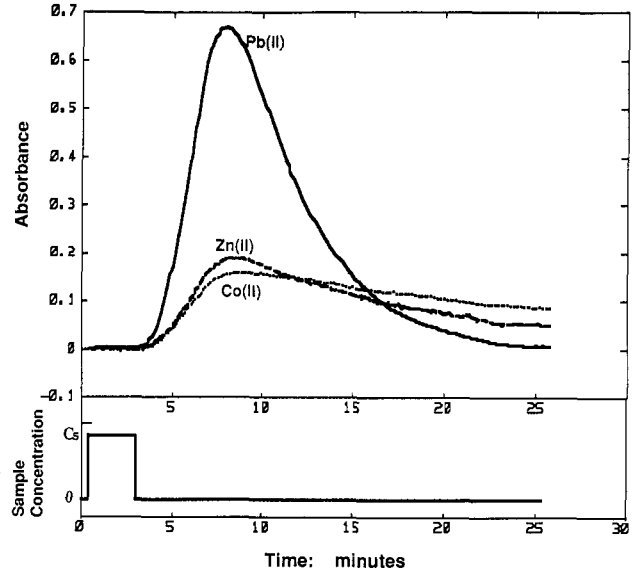

Figure 1. Elution profiles of different ions: Pb(II) concentration, 1.5 × 10^{-6} M; Co(II) and Zn(II) concentration, 3 × 10^{-6} M each; receiving solution, 0.1 M $Na_2S_2O_3$ in 0.05 M NaAC/HAC buffer solution; pH, 5.0.

THEORY

Temporal Species Discrimination. In this sensor, the temporal domain information is provided by the diffusion behavior of the metal ions through the Nafion cation-exchange membrane. Utilizing the specificity of $Na_2S_2O_3$ in complexation with metal ions, one can selectively increase the membrane-phase diffusivities and the concentration gradients of the targeted metal ions, Pb(II) and Cd(II). As the first step of permeation, partition of the transition metal ion into the cation-exchange membrane (sodium form) is a spontaneous process. Once in the membrane, Pb(II) and Cd(II) form neutral or negatively charged complexes with the thiosulfate ions that "invade"[16] into the membrane phase. These complexes are not retained by the functional groups of the cation-exchange membrane, resulting in the increased diffusivities of Pb(II) and Cd(II). The concentration gradients of the targeted ions are increased because the number of "free" ions capable of back-diffusion is dramatically reduced by the complexation. Thus, with a sample whose concentration changes in a Δ function (Figure 1), the elution profiles of Pb(II) and Cd(II) ions are relatively sharp peaks. Since other transition metal ions, considered the interfering ions here, are not favorable in complexation with $Na_2S_2O_3$: (1) their concentration gradients across the membrane are not increased and (2) they are retained by the functional groups of the cation-exchange membrane as they permeate through it. Therefore, the interfering ions can be distinguished from the targeted ions by their low peak height and tailing elution profiles. Figure 1 compares the elution profiles of the targeted ion, Pb(II), and interfering ions, Zn(II) and Co(II). As expected, the elution profiles of interfering ions have long tailing parts due to the slow ion-releasing processes from the membrane phase. Although the dialysis process is not completely selective to Pb(II) and Cd(II), it does create enough difference in the elution profiles for discrimination of Pb(II), Cd(II), and interfering ions in the temporal domain.

Spectral Species Discrimination. The eluted ions are detected spectroscopically as they react with a metal indicator, 4-(2-pyridylazo)resorcinol (PAR), to form orange-red metal ion–PAR chelates. PAR has been widely used as an indicator in colorimetric analysis of metal ions.[17] Like most metal indicators, PAR is not selective. Analysis by zero-order methods necessitates a tedious sample pretreatment process to remove the interferences.[18,19] Benefited by the second-order advantage, the sensor employed here requires only partial selectivity in spectral detection, which can be easily achieved by utilizing the different absorption peak shifts caused by the difference in electron structure among the various kinds of metal ion–PAR chelates. Figure 2 compares the second-derivative spectra of various kinds of chelates. In the visible region, as usual, the peaks are broad and heavily overlapped. However, the peak shifts are large enough for distinguishing different species. Note that spectral differences occur in the range of 460–600 nm.

Bilinearity Considerations. A fundamental requirement of GRAM and TLD is that the data must be bilinear. Such type of data matrix is generated by a bilinear instrument and can be decomposed into

$$\mathbf{N} = \mathbf{XCY}^{\mathrm{T}} = \sum_{k=1}^{K} (\mathbf{x}_k c_{k,k} \mathbf{y}_k^{\mathrm{T}}) \qquad (1)$$

where N is the bilinear matrix, X and Y are matrices whose columns $\mathbf{x}_k$ and $\mathbf{y}_k$ are vectors representing the pure constituent responses in the column space and row space of N. C is a

(11) Lin, Z.; Burgess, L. B. *Anal. Chem.*, preceding paper in this issue.
(12) Bond, A. M.; Hudson, H. A.; Luscombe, D. L.; Timms, K. L.; Walter, F. L. *Anal. Chim. Acta* **1987**, *200* (1), 213–25.
(13) Krzysztof, R. *Anal. Chim. Acta* **1993**, *273* (1–2), 485–92.
(14) Anuar, K.; Hamdan, S. *Talanta* **1992**, *39*, (12), 1653–6.
(15) Borracino, A.; Campanella, L.; Sammartino, M. P.; Tomassetti, M. T. *Sensors Actuators B* **1992**, *7*, 535–9.
(16) Rieman, W.; Walton, H. *Ion Exchange in Analytical Chemistry;* CRC Press Inc.: Boca Raton, FL, 1990.
(17) Marzenco. *Spectroscopic Detection of Elements;* John Wiley & Sons Inc.: New York, 1976.
(18) Yotsuyanagi, T.; Yamashita, R.; Aomura, K. *Anal. Chem.* **1972**, *44*, 1091–3.
(19) Nonova, D.; Evtimova, B. *Talanta* **1973**, *20*, 1347.

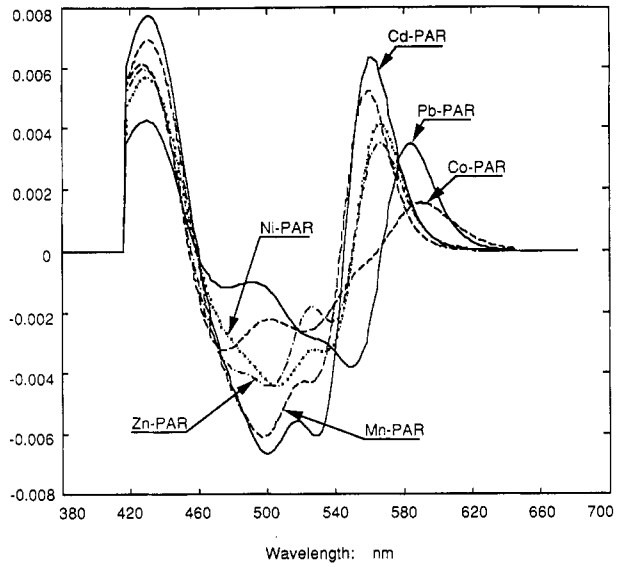

Figure 2. Second-derivative spectra of metal ion–PAR chelates. In 0.025 M $Na_2B_4O_7$/NaOH buffer + 0.077 M $Na_2S_2O_3$ + 0.038 M NaAC, pH = 10.5. PAR concentration, 3×10^{-4} M; blank, PAR solution.

diagonal matrix whose elements $c_{k,k}$ represent the concentration of the constituent in the sample. The superscript T stands for the transpose of a vector or a matrix. In the sense of instrumentation, the mathematical expression means that, as a bilinear device, the response profiles in both domains of the instrument arising from a species should be unique, consistent, and independent of the presence of other species. By this definition, this second-order sensor can be considered as a bilinear device. In the temporal domain, the transport behavior of each ion is independent of the others, because the sensor works in a low concentration range where the interaction among the ions is very small. In the spectral domain, the chelated species are stable during the time of mixing and detection. There is no further reaction involved with the chelated species inside the sensor. The indicator forms a 1:1 or 2:1 (PAR:ion) chelated species with a metal ion, depending upon the pH of the mixed solution.[20] Once the pH is stabilized by buffering the indicator solution, speciation of the chelate–metal ion system is consistent so the spectral peak for each metal ion will not vary with the time.

Second-Order Data Analysis. Generalized rank annihilation method (GRAM) and trilinear decomposition (TLD) are second-order calibration algorithms which do not require any assumption of physical profiles to provide unique resolutions. The theories of these methods have been discussed by Sanchez, Wilson, and Kowalski.[3,21,22] Provided here is a summary of GRAM for quick reference to the key steps of the algorithm. Since TLD can be viewed as an extension of GRAM, the introduction of this method will be very brief and for the purpose of comparing the difference between TLD and GRAM. The theoretical discussion of the TLD method may be found in ref 22.

(1) GRAM. In GRAM, a single standard is used for calibration, and the analyte concentration in one sample is predicted. Information in both standard and sample data matrices is combined by concatenating the sample data matrix, $\mathbf{M}(I \times J)$, and the standard data matrix, $\mathbf{N}(I \times J)$. The two concatenated matrices are subject to decomposition by singular value decomposition (SVD):

$$\frac{\mathbf{M}}{\mathbf{N}} = \mathbf{U}\mathbf{S}_1\mathbf{Q}^T \tag{2}$$

$$\mathbf{M}\|\mathbf{N} = \mathbf{P}\mathbf{S}_2\mathbf{V}^T \tag{3}$$

Once the number of principle components (PC) K is chosen, the first K columns of the loading matrix $\mathbf{P}$ of $\mathbf{M}\|\mathbf{N}$, denoted as $\bar{\mathbf{P}}(I \times K)$, defines the common row space. The first K columns of the score vector $\mathbf{Q}$ of $\underline{\mathbf{M}}/\mathbf{N}$, denoted as $\bar{\mathbf{Q}}(J \times K)$, defines the common column space.

The common spaces cover the variations in both standard and sample data matrices. $\mathbf{S}_1$ and $\mathbf{S}_2$ are the matrices of singular values. The standard and sample data matrices are then projected into the common row and column spaces:

$$\mathbf{M}_{PQ} = \bar{\mathbf{P}}^T\mathbf{M}\bar{\mathbf{Q}} \tag{4}$$

$$\mathbf{N}_{PQ} = \bar{\mathbf{P}}^T\mathbf{N}\bar{\mathbf{Q}} \tag{5}$$

The square matrices $\mathbf{M}_{PQ}$ and $\mathbf{N}_{PQ}$ fit into the generalized eigenproblem:

$$\mathbf{M}_{PQ}\mathbf{Z} = \mathbf{N}_{PQ}\mathbf{Z}\Lambda \tag{6}$$

Using the QZ algorithm to solve the eigenproblem, we obtain the eigenvalue matrix Λ, which contains the concentration ratios:

$$\Lambda = \mathbf{C}_M(\mathbf{C}_N)^{-1} \tag{7}$$

where $\mathbf{C}_M$ and $\mathbf{C}_N$ are the diagonal concentration matrices of the mixture sample and the standard, respectively.

Determination of the proper number of principal components (PC) is a critical step in building up a calibration model. This is usually done by cross-validation of the data matrix. In ref 23, a series of predicted residual sum of squares (PRESS) are obtained as the result of using different number of factors. In theory, the optimal number of factors (hence the PCs) is obtained when PRESS hits the minimum. In practice, however, the noise carried by the less significant factors might cause complex eigensolutions of eq 6. Therefore, sometimes using less PCs than the optimal number is preferred in order to avoid complex solutions. The lower limit of the number of PCs used in the model is that the information of the analytes must be well modeled. Fitting the calculated elution profiles and spectra of the pure analytes to the measured ones and calculating the root mean square errors (RMSE)[24] can be used as a quatitative means of judgment. For an acceptable model, the RMSE of curve fitting should be less than or

(20) Cheng, K. L., Ueno, K., Imamura, K., Eds. *CRC Handbook of Organic Analytical reagents;* CRC Press, Inc.: Boca Raton, FL; pp 195–201.
(21) Wilson, B. E.; Sanchez, E.; Kowalski, B. R. *J. Chemom.* **1989**, *3*, 493–8.
(22) Sanchez, E.; Kowalski, B. R. *J. Chemom.* **1990**, *4*, 29–45.
(23) D'Amboise, M.; Lagarde, B. *Comput. Chem.* **1989**, *13* (1), 39–44.
(24) Malinowski, E. R. *Factor Analysis in Chemistry*, 2nd ed.; John Wiley & Sons: New York, 1991; pp 117–20.

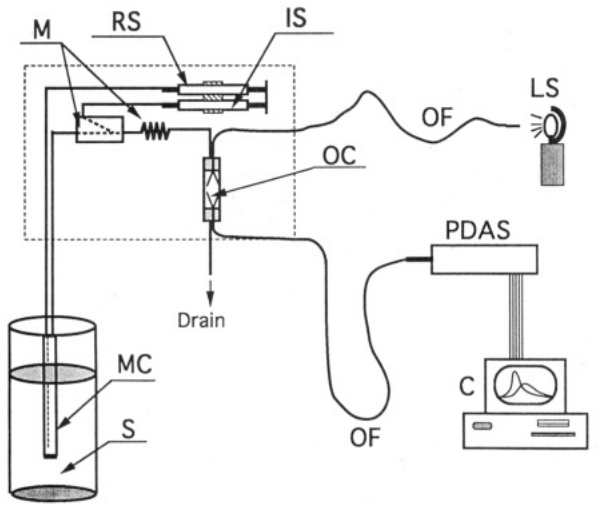

Figure 3. Sensor configuration: C, computer; IS, indicator syringe; RS, receiving solution syringe; LS, light source; OC, optical cell; OF, optical fiber; M, mixer and mixing coil; MC, membrane cell; PDAS, photodiode array spectrometer; S, sample.

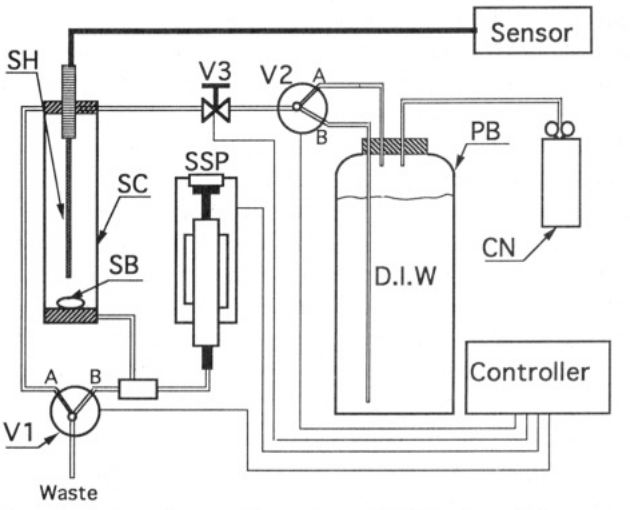

Figure 4. Automatic sampling system: V1–V3, valves; SH, sensor head; SC, sampling cell; PB, pressurized bottle; DIW, deionized water; CN, compressed nitrogen; SSP, sample syringe pump; SB, stirring bar.

comparable to the sensor noise. The calculated matrix of elution profiles is

$$\hat{\mathbf{Y}} = \bar{\mathbf{Q}}(\mathbf{Z}^{+})^{\mathrm{T}} \tag{8}$$

and the matrix of calculated spectra is

$$\hat{\mathbf{X}} = \bar{\mathbf{P}}(\mathbf{N}_{\mathrm{PQ}} + \mathbf{M}_{\mathrm{PQ}})\mathbf{Z} \tag{9}$$

Since the calculated and measured profiles and spectra are in arbitrary scales, scaling is necessary to make any comparison.

(2) TLD. A major advantage of TLD over GRAM is that TLD uses multiple standards. Therefore, a statistically better prediction can be obtained over a given concentration range, and the prediction is less affected by the measurement errors. In TLD, common row (temporal), column (spectral), and "tube" (sample) spaces are found by computing the SVD of the concatenated second-order data matrices obtained from unfolding the three-dimensional data cube along each order. Only the first two columns of the joint tube space are retained to construct two pseudo-sample data matrices, which are the linear combination of all standard and sample data matrices. These pseudo-sample data matrices are projected into the common row and column spaces so that two generalized eigenvalue–eigenvector equations can be established. By solving the eigenproblems, calculated physical profiles (e.g., elution profile and spectrum) can be obtained. TLD uses the least square fit of the calculated physical profiles to calculate the concentrations of pure constituents.

EXPERIMENTAL SECTION

Experiment Setup. The sensor is schematically illustrated in Figure 3. The dialysis cell is a piece of one-end-plugged tubular Nafion cation-exchange membrane into which a piece of polymer-coated silica capillary has been inserted. This capillary delivers the receiving solution and increases the surface-to-internal volume ratio of the dialysis cell. As the receiving solution flows through the cell, eluted metal ions are brought to a mixing channel where they mix and react with the metal indicator, 4-(2-pyridylazo)resorcinol. The metal ion–PAR chelates are then brought into the fiber optic flow cell for detection. The detailed specifications of dialysis cell, mixing channel, reagent delivering pump, fiber optic detection cell, and dialysis process are given in ref 11. The optical cell is illuminated by a tungsten light source coupled with a source fiber (200-mm core, glass on glass, NA = 0.21). The transmission signal is collected by the same type of fiber and delivered into a portable diode array spectrometer (SD1000, Ocean Optics, Inc.) A SMA connector couples the signal fiber to the spectrometer. The spectral coverage of the spectrometer is from 400 to 650 nm with a resolution of 3 nm if a 50-mm core fiber is used. The data acquisition software delivered with the spectrometer was modified so that it can be used to continuously collect the spectra at a prescribed interval.

An automated sample delivery system is used to insure precise sample deposition time. Figure 4 shows the schematics of the system. Purging and refilling the sampling cell is accomplished using the pressurized bottle. The valves (Slider Valve 5301, Rheodyne, Inc.) and the sample injecting syringe pump (50 SMB2-HM, Aerotech, Inc.) are controlled by a programmable controller (UNIDEX 11, Aerotech, Inc.). The solenoid valve kits for pneumatic operation of the slider valves are from Rheodyne, Inc. (Model 7163).

Materials and Reagents. Nafion tubular membrane (1100 EW, 610 mm I.D., 100 mm wall thickness) was obtained from Perma Pure Products, Inc. Metal indicator 4-(2-pyridylazo)-resorcinol (PAR) was purchased from Aldrich Chemical Co. Sodium borate, sodium thiosulfate, sodium acetate, and acetic acid (aldehyde free) are analytical grade and were obtained from Baker Inc. Sodium hydroxide solution was purchased from VWR. All nitrates of Pb(II), Cd(II), Ni(II), Mn(II), Co(II), and Zn(II) are analytical grade and were obtained from Aldrich Chemical Co.

Procedures. The receiving solution is prepared by dissolving 12.4 g of sodium thiosulfate into 500 mL of sodium acetate–acetic acid buffer. The buffer contains 0.05 M sodium acetate and the required amount of aldehyde-free acetic acid to adjust

the pH to 5.1. At this pH, the complexation of acetate with analyte ions is weak. Therefore, the interference to thiosulfate complexation is negligible. The indicator solution is prepared by adding 0.059 g of PAR into 250 mL of sodium borate buffer. The buffer of pH 10.8 is prepared by mixing 125 mL of 0.1 M sodium borate solution and 60.6 mL of 0.4 M NaOH and diluting it to 250 mL with distilled deionized (DI) water. The sample solutions are prepared by diluting the stock solutions, which are prepared from the metal nitrates. The pH of sample solutions is in the range of 5.6–5.9, depending on the pH of the DI water. The real-world samples are tap water and the Lake Union water collected near the campus. The pH values are 5.5 and 5.2 for the tap water sample and Lake Union sample, respectively.

Each measurement consists of a 30-min cycle, starting with purging the sampling cell with compressed N_2 (valve 1 at position B, valve 2 at position A, valve 3 open) and then injecting the sample (valve 1 at position A, valve 3 closed, sample syringe pump on). After a 150-s sample deposition, compressed N_2 purges the cell again. Then the cell is refilled with DI water (valve 1 at position A, valve 2 at position B, valve 3 open). This purging–refilling cycle is repeated three times for cleaning the residual sample. The data collection interval is set to 24 s. The integration time of the spectrometer is 0.01 s. For each spectrum taken, 50 scans are averaged.

RESULTS AND DISCUSSION

Evaluation of Sensor with SVD. The responses to pure analyte [Pb(II)] and a mixture containing Pb(II) and interferents [Co(II), Mn(II), Ni(II), and Zn(II)] are shown in Figure 5 as the examples of second-order data. Second-derivative spectra are used throughout the following analysis in order to amplify the spectral differences and minimize the base line drift. It is very clear that there are spectral differences between the pure Pb(II) and the mixture data. The temporal difference between two data sets can also be observed. Unlike the Pb(II) signal, the signal of the interferent mixture does not go back to the base line because of the slow releasing process of the interferents from the membrane. Principal component analysis is used to model the responses by several significant orthogonal vectors (PCs). Singular value decomposition (SVD) is one of the algorithms to calculate the orthogonal vectors.[24] Briefly speaking, SVD decomposes a data matrix into two normalized matrices, loading matrix and score matrix, respectively, and a diagonal matrix containing singular values, each of them indicating the amount of variance in a corresponding vector. For the second-order data of the sensor, the loading vectors in the loading matrix describe the spectral information whereas the score vectors depict the elution profiles of different ions. In Figure 6A, the first loading vector from the Pb(II), Co(II), Mn(II), Ni(II), and Zn(II) mixture data mainly describes the combined spectra of the interferents. Because of the similarity in their elution profiles, the interferences are collinear and cannot be separated into several corresponding orthogonal vectors. The variance of the Pb(II) signal can be primarily described by the second loading vector due to the substantial difference between its elution profile and those of the interferents. The third loading vector in Figure 6B is mainly associated with the variance of the mixed reagent solution. The large variance around 450

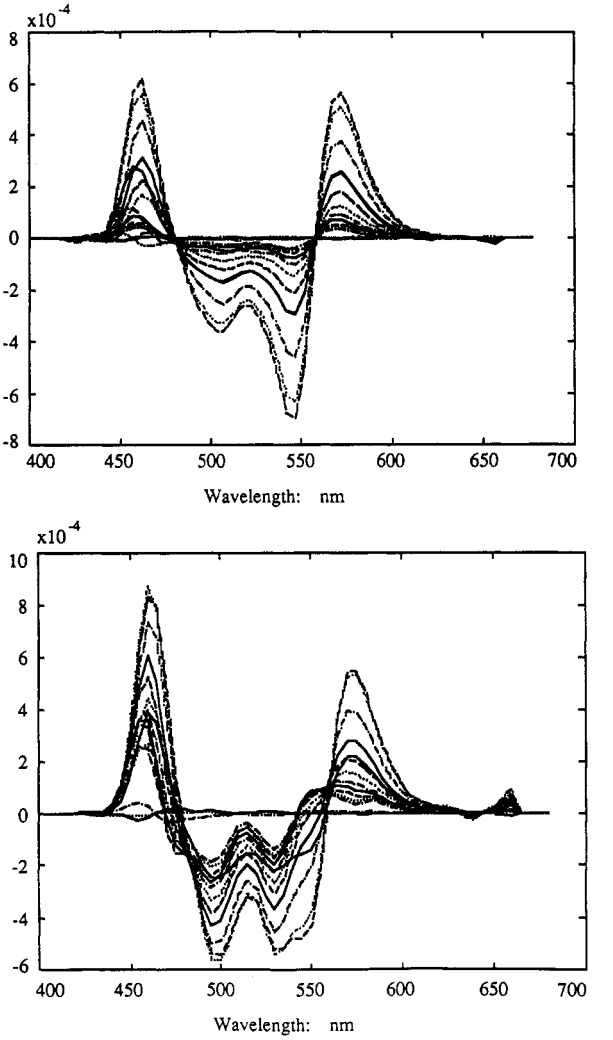

Figure 5. Response of the second-order sensor to (A) pure Pb(II), 1.5×10^{-6} M and (B) Pb(II), 1.5×10^{-6} M with interferent ions: Co(II), Mn(II), Ni(II), and Zn(II), 0.5×10^{-6} M each.

nm is due to consumption of the indicator by the eluted ions. There is a small signal in the 540–580-nm region of the third loading vector. This corresponds to the Pb(II) signal. The fourth loading vector contains some residual spectral signal. The score vectors are shown in Figure 7. The first score vector obviously corresponds to the combined elution profiles of the interferents, as it has the characteristic tail. The elution information of these interfering ions is described by a single score vector because of the similarity in their diffusion behaviors. The elution profile of Pb(II) is described by the second score vector. This vector is also associated with some reagent mixing noise and the variance caused by metal indicator consumption. The mixing noise shows up primarily on the third and fourth score vectors, as shown in Figure 7B. The periodic noise is from inconsistent movement of two delivery syringes. Since the internal volume of the sensor's mixer is very small, the mixing ratio is very sensitive to this type of inconsistency. One method to reduce the fluctuation is to put a filter on each of the syringes to increase the flow resistance so that the inconsistent movement can be absorbed in some degree by the elasticity of the syringes.

As in the Pb(II) data, information about the interferents is embedded in the first factor of the Cd(II) data. Information

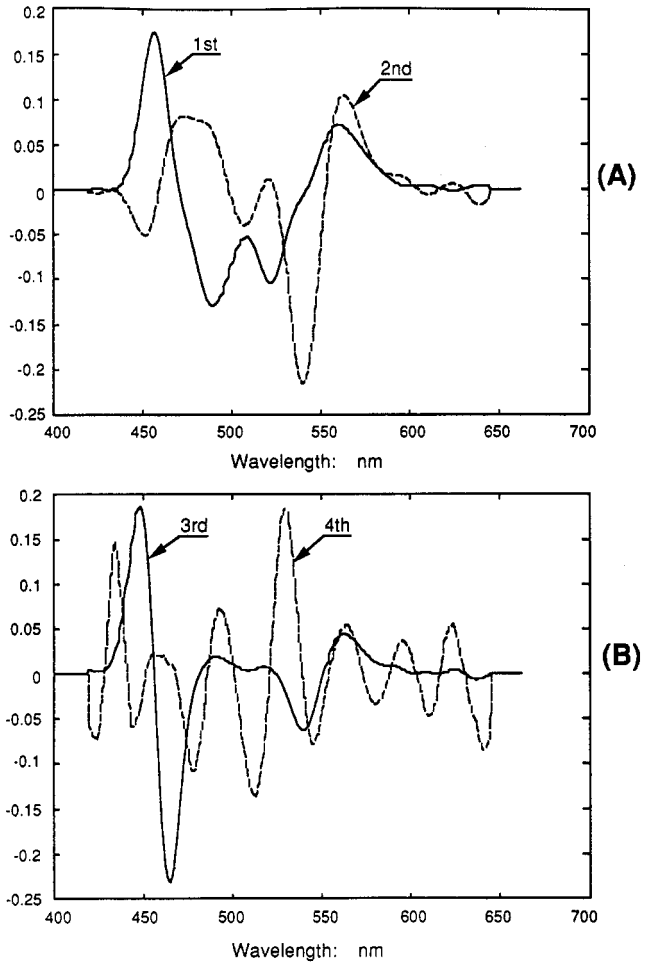

Figure 6. Singular value decomposition (SVD) loadings of mixture data: Pb(II) (1.5×10^{-6} M) with Co(II), Mn(II), Ni(II), and Zn(II) (0.5×10^{-6} M each).

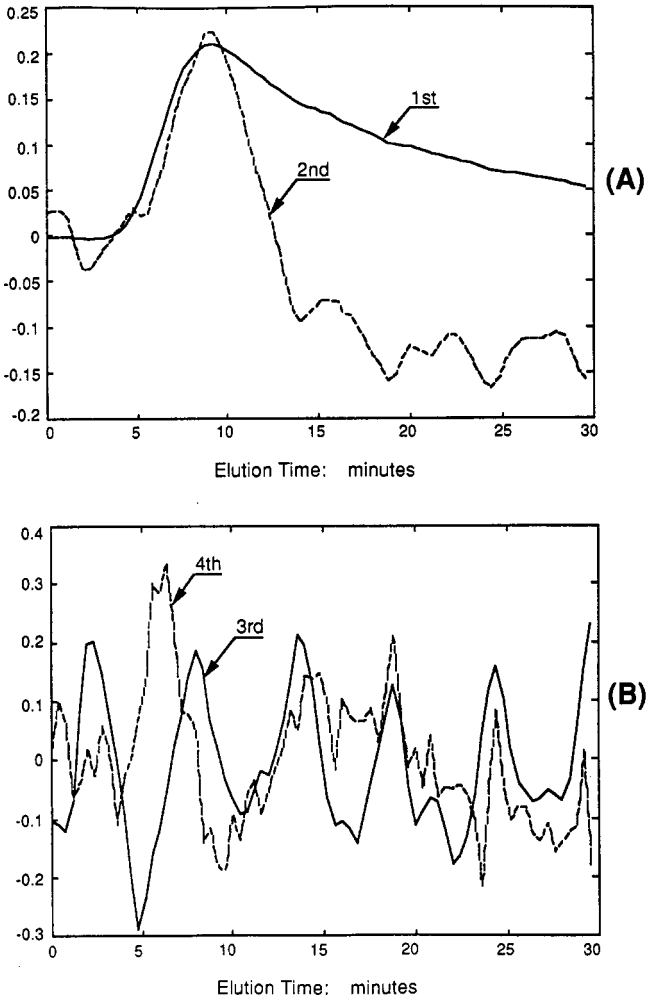

Figure 7. Singular value decomposition (SVD) scores of mixture data: Pb(II) (1.5×10^{-6} M) with Co(II), Mn(II), Ni(II), and Zn(II) (0.5×10^{-6} M each).

of Cd(II) is mainly represented by the second factor. Because the absorbance peak of the Cd–PAR chelate is close to that of PAR, more relevant information is embedded in the third factor, making it significant enough to be included in the model. Variance due to indicator consumption is distributed in the second and the third factors. The fourth factor mainly describes mixing noise. Because of the similarity in the pattern of the principal components of Pb(II) and Cd(II) data sets, the loadings and scores of the Cd(II) data set will not be illustrated here.

Measurement of Artificial Samples. The samples are prepared by fixing the concentrations of the interferents [Co(II), Mn(II), Ni(II), and Zn(II), 0.5×10^{-6} M each] and varying the concentration of the analyte, Pb(II) or Cd(II). A series of standards containing pure Pb(II) or Cd(II) are measured for the prediction. The number of PCs is determined by cross-validation of the concatenated (by columns) data set of the samples. The PRESS values in Figure 8 indicate that the optimal numbers of PCs for Pb(II) and Cd(II) data are three and four, respectively, which are less than the number of chemical components in the samples due to the similarity in the elution profiles of the interfering ions. In order to completely avoid complex solutions, two PCs are used in Pb(II) calibration and three are used in Cd(II) prediction. A small percentage of analyte information may be left out of the models by reducing the PC numbers by one, but in this study

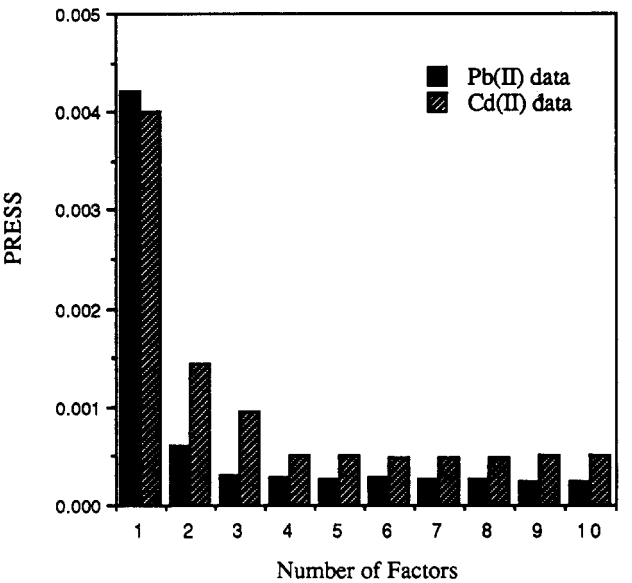

Figure 8. Root mean square errors of cross-validation of Pb(II) and Cd(II) data [containing interferences of Co(II), Mn(II), Ni(II), and Zn(II)] using various number of factors.

the consequent errors are smaller than including the last PC with its associated errors. The models are then verified by comparing the calculated elution profiles and spectra of Pb(II) and Cd(II) using GRAM with the measured ones. Figure

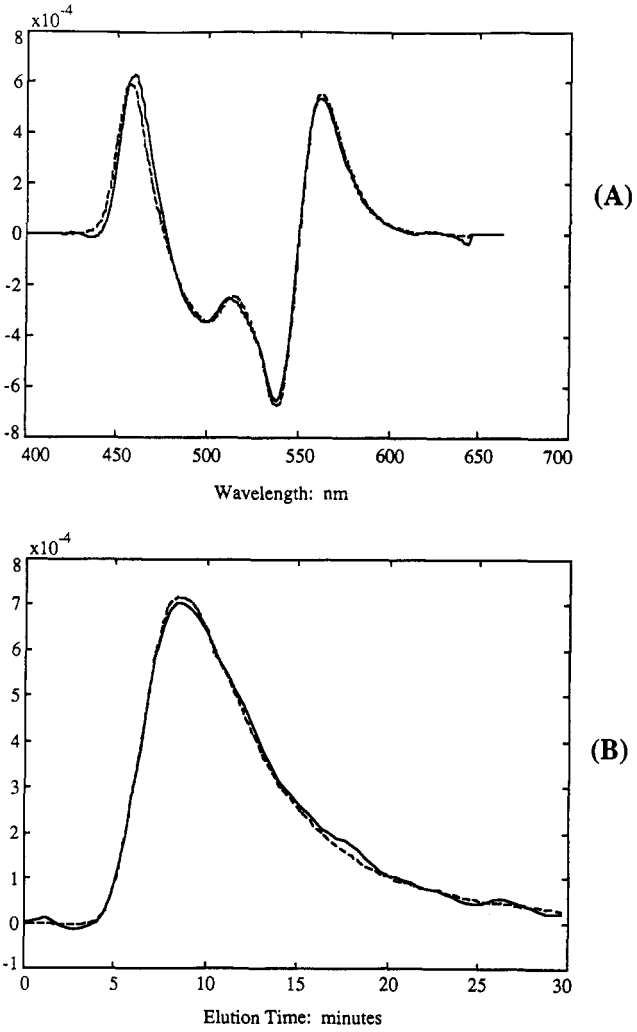

Figure 9. Comparison of the spectrum and the elution profile of Pb(II) with the calculated ones with GRAM: (A) spectra; (B) elution profiles; (—) measured; (- - -) calculated with GRAM.

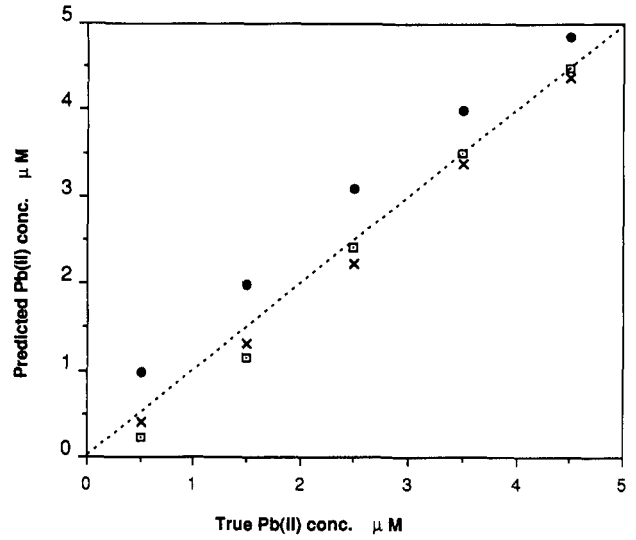

Figure 10. Comparison of the results of Pb(II) prediction using GRAM, TLD, and univariate method (526 nm): (- - -) theoretical prediction line; (⊡) GRAM results; (×) TLD results; (●) single wavelength results; interfering ions: Co(II), Mn(II), Ni(II), and Zn(II), 0.5 × 10^{-6} M each; standard deviation, 0.077 × 10^{-6} M.

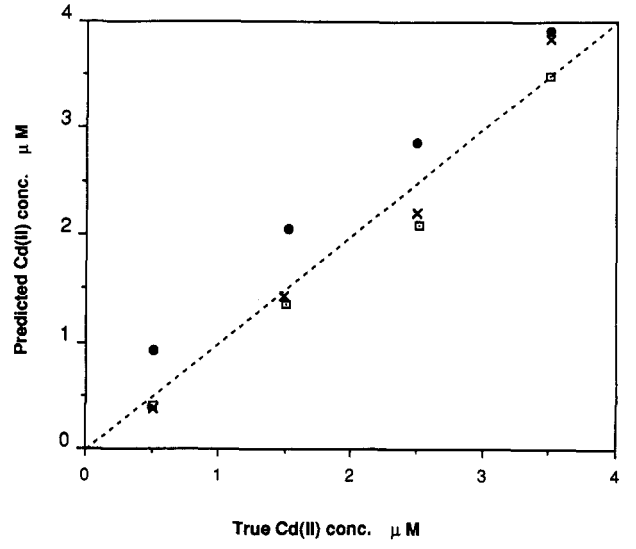

Figure 11. Comparison of the results of Cd(II) prediction using GRAM, TLD, and univariate method (526 nm): (- - -) theoretical prediction line; (⊡) GRAM results; (×) TLD results; (●) single wavelength results; interfering ions: Co(II), Mn(II), Ni(II), and Zn(II), 0.5 × 10^{-6} M each; standard deviation, 0.081 × 10^{-6} M.

9 shows the comparison of Pb(II) elution profiles and spectra as an example, in each case a scaling constant is adjusted to minimize the RMSE of curve fitting. The RMSEs of spectra and elution profile fitting are 3.21 × 10^{-7} and 9.45 × 10^{-9} absorbance units (second-derivative spectra), respectively, both comparable with the sensor noise level of 2.88 × 10^{-7} absorbance units (second-derivative spectra). Figures 10 and 11 compare the prediction results using second-order calibration methods (GRAM and TLD) and zero-order method (single wavelength, monovariate). It is easy to see that the measurements are biased if the single wavelength (zero-order) approach is used. Since the concentrations of the interferents are fixed, the results of single wavelength detection show a constant positive offset from the true values. When the second-order approaches are used, the positive bias is removed. However, there are considerably large errors in GRAM prediction results using the full-size data (full elution profile, see Table 1). There are two major factors to cause the error. The first is the competition of co-existing cations (all other cations except the analyte in the solution) with the analyte in the ion-exchange process on the membrane surface.[11] Since the process does not reach equilibrium during the short sensor exposure time, the amount of analyte ions partitioned in the membrane phase is predominately determined by the probability of the analyte ions to contact with the functional groups at the membrane surface. The competition of co-existing ions reduces the probability and, hence, the sensor response to the analyte. This effect is not significant when analyte concentrations are high relative to those of co-existing ions, but not negligible when the analyte concentrations are relatively low

Table 1. Errors of Pb(II) Prediction with GRAM Using Full-Size Data[a]

stds, Pb(II), 10^{-6} M	samples, Pb(II), 10^{-6} M, plus interfering ions				
	0.5 (%)	1.5 (%)	2.5 (%)	3.5 (%)	4.5 (%)
0.5	*-44.5*	-7.9	-59.8	119.6	155.0
1.5	-52.2	*-11.7*	5.9	20.8	22.7
2.5	-61.6	-25.0	*-6.4*	7.7	9.1
3.5	-66.2	-32.0	-13.7	*2.8*	4.7
4.5	-70.2	-37.7	-19.7	-0.5	*3.6*

[a] Interfering ions: Co(II), Mn(II), Ni(II), Zn(II), 0.5 μM each.

Table 2. Errors of Pb(II) Prediction with GRAM Using Truncated Data[a]

stds, Pb(II), 10^{-6} M	samples, Pb(II), 10^{-6} M, plus interfering ions				
	0.5 (%)	1.5 (%)	2.5 (%)	3.5 (%)	4.5 (%)
0.5	*-57.0*	-23.3	-7.8	-2.1	-3.0
1.5	-50.4	*-11.9*	4.1	5.0	3.8
2.5	-55.4	-19.7	*-1.3*	-0.9	-0.3
3.5	-56.0	-25.4	-2.2	*-1.2*	-1.3
4.5	-55.8	-19.3	0.0	1.5	*1.7*

[a] Interfering ions: Co(II), Mn(II), Ni(II), Zn(II), 0.5 μM each.

Table 3. Errors of Cd(II) Prediction with GRAM Using Truncated Data[a]

stds, Cd(II), 10^{-6} M	samples, Cd(II), 10^{-6} M, plus interfering ions			
	0.5 (%)	1.5 (%)	2.5 (%)	3.5 (%)
0.5	*-18.1*	0.5	-13.5	21.5
1.5	-3.5	*-7.2*	19.7	-1.3
2.5	-11.2	-7.3	*-19.2*	-1.7
3.5	-67.9	-23.5	-14.1	*0.0*

[a] Interfering ions: Co(II), Mn(II), Ni(II), Zn(II), 0.5 μM each.

Table 4. Errors of Pb(II) and Cd(II) Prediction with TLD Using Truncated Data

stds, Pb(II), 10^{-6} M	samples, Pb(II), 10^{-6} M, plus interfering ions				
	0.5 (%)	1.5 (%)	2.5 (%)	3.5 (%)	4.5 (%)
0.5, 1.5, 2.5, 3.5, 4.5	-14.6	-9.3	-11.1	-3.2	-4.6
stds, Cd(II), 10^{-6} M	samples, Cd(II), 10^{-6} M, plus interfering ions				
	0.5 (%)	1.5 (%)	2.5 (%)	3.5 (%)	
0.5, 1.5, 2.5, 3.5	-15.7	-1.2	-12.8	13.6	

Table 5. Pb Analysis of Tap Water and Lake Water Samples[a]

sample	sensor results (μg/L)				verification with GFAA (μg/L)	
	GRAM		TLD			
	av	SD	av	SD	av	SD
tap water	6.5	1.6	6.3	0.9	6	0.5
Lake Union water	5.7	2.3	5.5	1.2	10	0.4

[a] Sample pH: 5.5 for tap water and 5.2 for the lake water.

or the affinities of co-existing ions to the membrane are high. This can be observed from the data on the diagonal line in Table 1 (italics). The negative bias at the low analyte concentrations clearly indicates that less analyte ions can partition in the membrane when there are other cations in the sample. The second factor is the nonlinearity of sensor response. As a linear method, GRAM relies on the linearity of the device to make good prediction over a range of concentrations. Deviation from the ideal linearity introduces extra error when the standard and sample concentrations are different. This is revealed by the off-diagonal line data in Table 1, where the prediction error is increased when using a low concentration standard to predict high concentration samples and vice versa.

For this particular sensor, it is found that the response linearity can be improved by truncating the rising part of the elution profile from the data set (removing the first 24 scans of the data file). The rising part of the elution profile contains little chemical information to distinguish the ions, as shown in Figure 1, where the rising parts of the elution profiles of different ions are similar. The results in Table 2 and Table 3 show smaller error than that of using the full-size data, especially when the standard and sample concentrations are different (see the rows in the tables). The remaining negative bias at low analyte concentrations is mainly attributed to the competition effect of the co-existing ions in the samples and cannot be corrected by the data truncation. However, when the analyte concentration is very low so that signal saturation will not occur, this competition effect can be reduced by using longer sensor exposure time so that the ion-exchange process is close to the equilibrium where the amount of analyte ion partitioning in the membrane is predominately determined by its affinity to the membrane phase.

It is obvious that the nonlinearity problem can be circumvented by using a standard whose concentration is close to that of the sample. In real applications, however, choosing a "close" standard concentration may not be trivial. In this regard, TLD is superior to GRAM because it uses least square fit based on the calculated elution profiles and spectra from multiple samples to obtain statistically better prediction within a given concentration range. From Table 4, one can see that TLD reduces prediction errors in low concentration mixtures, especially for Pb(II). TLD is most effective if the response curve is basically linear but imposed by random noise. It cannot handle large nonlinearities, such as in the case of using full-size data sets of Pb(II) and Cd(II). For this reason, an extended TLD algorithm with nonlinear curve fitting techniques is developed to improve the capability of handling the nonlinearities. This method will be described in the following paper.[25]

Measurement of Real-World Samples. Real-world sample matrices are more complicated. They may contain species that can cause spectral peak distortion by affecting the chemical condition of metal ion–PAR chelating process. In this case, the Donnan dialysis process not only provides time domain information for the sensor but also reduces the matrix effect by screening out anionic ions and large neutral species. In this experiment, two types of real-world samples, tap water and lake water (Lake Union water samples), were analyzed for Pb(II) concentration. Four standards containing 4–7 × 10^{-8} M $Pb(NO_3)_2$ (1 × 10^{-8} M increment) were used in TLD prediction. GRAM used the 5 × 10^{-8} M $Pb(NO_3)_2$ solution as the standard. To increase the sensor's sensitivity, stopped-flow measurement was used. While the sample was stirred, the receiving solution was stopped for 8 min to accumulate the ions. The long accumulation time also minimizes the competition effect of the co-existing ions. After preconcentration, the flow was resumed for detection. Five consecutive measurements were carried out for each sample. Before calibration, the first 24 spectra were truncated from each data matrix because, in this part of the data matrix, the temporal variances of different ions were collinear due to the stopped-flow accumulation. Table 5 lists the Pb(II) concentrations and standard deviation of sensor measurement with GRAM and TLD calibration. For verification, Pb analysis using graphite furnace atomic absorption (GFAA) was carried out, and the results are also listed. The sensor data shows

(25) Booksh, K. S.; Lin, Z.; Wang Z.; Burgess, L. W.; Kowalski, B. R. *Anal. Chem.*, following paper in this issue.

very good agreement with that of GFAA in tap water measurement. The lowest limit of detection of the GFAA is 3 ppb. It has been found by ICP-AES that the tap water sample contains 449 ppb of Cu and 45 ppb of Zn ions. These are significantly higher than the concentrations of other transition metal ions. The predicted Pb(II) concentration in the Lake Union water sample from this sensor, however, is much lower than that from GFAA. Since the pH values of both the tap water sample and the Lake Union water sample were almost the same, this difference must be attributed to the complexation of Pb ions with the organic species in the lake water. Because the membrane does not favor permeation of large neutral or negatively charged species, the sensor only measures the free Pb ions, which is a fraction of the total Pb concentration measured by the atomic spectroscopic methods.

CONCLUSION

Under the chosen parameters of the dialysis process and metal ion indicator complexation, elution profiles and spectra of analyte and interfering ions are significantly different. This enhances the resolution of analyte information from the interference. The cation-exchange membrane functions well in all measurements, partially because the membrane is immersed in the blank solution for most of the time so its original condition is preserved. In general, this sensor is promising to be developed into low-cost, selective, and versatile instruments for in situ, distributed measurement of heavy metals. The second-order sensor design can also be used as a platform of second-order in situ devices for measuring other species. There are several aspects of the sensor that require continuous research. First, the error of prediction is large when the standard and sample concentrations are very different. Research of the dialysis system, especially the facilitated ion-exchange process, is necessary in order to improve the sensor linearity. Developing second-order calibration algorithms that have nonlinear curve fitting capability is equally important to improve the sensor linearity. Second, the analysis time of the sensor is considerably long compared to other instruments. The current sensor is not optimized in the engineering point of view. The membrane thickness, the size of the dialysis cell, and the internal (void) volume of the sensor should be reduced so that the elution time and the lag time could be minimized. Finally, like all sensors using an ion-selective technique, the sensor's response is affected by speciation of the analyte. Acidifying the sample will release the complexed ions to obtain "total" concentration of the analyte. In this particular case, however, sample acidification was limited by the small complexation capability of the thiosulfate ion and its instability in acidic environment. The sensor response has a significant decrease when the sample pH was set to 3.0. A white sulfur layer from decomposition of thiosulfate is observed on the surface of the membrane. This problem can only be solved by finding another complexing reagent whose pK_a is close to 3.0.

ACKNOWLEDGMENT

The authors would like to thank Dr. David Veltkamp for his help in modifying the data acquisition software. Ms. Sherry Xu of Laucks Testing Lab. Inc. of Seattle is thanked for her verification of the sensor data with atomic absorption methods. Dr. Yongdong Wang's contribution to the sensor calibration is also appreciated. This work was supported by the Center for Analytical Chemistry (CPAC), a National Science Foundation Industry/University Cooperative Research Center at the University of Washington.

Received for review October 19, 1993. Accepted May 4, 1994.®

® Abstract published in *Advance ACS Abstracts,* June 15, 1994.